IEEE Access
Multidisciplinary | Rapid Review | Open Access Journal

Received 21 February 2023, accepted 28 March 2023, date of publication 10 April 2023, date of current version 14 April 2023.

Digital Object Identifier 10.1109/ACCESS.2023.3265955

RESEARCH ARTICLE

Feasibility Study on Online Diagnosis of Aging and Deterioration of Medium Voltage (MV) Three-Core Cable Based on Impedance Spectroscopy

MINGZHEN LI[1,2], (Member, IEEE), RUIJUN YUAN[3], JIE CHEN[4], LIBIN HU[4], CHENYING LI[4], LINGZHI WANG[5], AOWEI GUO[1], ANLI CHEN[1], AND XINSONG ZHANG[1]

[1]School of Electrical Engineering, Nantong University, Nantong 226019, China
[2]School of Electrical Engineering and Automation, Wuhan University, Wuhan 430072, China
[3]State Grid Nantong Electric Power Supply Company Ltd., Nantong 226000, China
[4]State Grid Jiangsu Electric Power Company Electric Power Research Institute, Nanjing 211103, China
[5]State Grid Quanzhou Electric Power Supply Company Ltd., Quanzhou 362000, China

Corresponding author: Mingzhen Li (mzli@ntu.edu.cn)

This work was supported in part by State Grid Corporation of China under Grant 5700-202118195A-0-0-00.

ABSTRACT In order to explore the feasibility of impedance spectroscopy in the application of online diagnosis of aging and deterioration of medium voltage (MV) three-core cables, based on the theory of transmission line equation, an aging and deterioration model of the MV three-core cable has been established. The impedance spectroscopy of the cable head-end under healthy and different aging and degradation states has been simulated and analyzed. Further, the effects the extent of aging, local deterioration size and position, line length, load rate and other factors on the impedance spectroscopy have been studied. According to the influence of the various factors on the impedance spectroscopy, a set of aging and deterioration diagnosis procedures and methods are proposed. The simulation results indicate that the state of the cable can be divided into 4 categories of ''healthy,'' ''overall aging,'' ''large-size deterioration'' and ''small-size deterioration.'' The impedance spectroscopies of different states have certain characteristics. These characteristics can be determined by specific criterion indicators such as the monotonous decrease of the value of the resonance peaks and the phase amplitudes, the value of the resonance peaks, and the eigen propagation frequency, etc. Therefore, impedance spectroscopy has broad application prospects for online diagnosis of aging and deterioration of MV three-core cable.

INDEX TERMS Power cable, aging and deterioration, online diagnosis, impedance spectroscopy.

I. INTRODUCTION

In recent years, power cables have been widely used in various fields of power transmission and distribution due to the excellent electrical properties. With the increase of service time, failures caused by cable aging and/or deterioration gradually increase [1], [2], [3]. Online monitoring of the insulation is of great significance for formulating maintenance and replacement plans and ensuring safe power supply. Compared with power-transmission cables, power-distribution cables are larger in number and have more complex geometries, which brings challenges to cable insulation testing [4], [5], [6].

There are many traditional insulation test methods, including insulation resistance test, voltage withstand test, material chemical test, dielectric loss test, partial discharge test, etc. Among them, the insulation resistance test [7] and the voltage withstand test [8] are both offline tests, and the basic principles are relatively simple. Both test the insulation performance by applying voltage between the core and the ground. The insulation resistance test is to reflect the insulation performance through the value of the insulation resistance, while

The associate editor coordinating the review of this manuscript and approving it for publication was Mehrdad Saif.

the voltage withstand test is to test whether the insulation will be broken down by applying 1.5 to 2 times the operating voltage to the insulation. These two methods are relatively rough and cannot accurately reflect the condition of the insulation. Material chemical test techniques, including oxidation induction time (OIT) and Fourier Transform Infrared Spectroscopy (FTIR), are relatively professional, and the results are relatively more accurate [9], [10]. However, this type of method requires slice sampling of insulating materials, which is a destructive test and cannot be monitored online. The dielectric loss test mainly reflects the energy loss of insulating materials under the action of alternating current (AC) by measuring the dielectric loss angle ($\tan\delta$), which is an important criterion for the degree of aging [11]. Currently, the value of $\tan\delta$ can be obtained either through offline testing or online monitoring [12]. The method of online monitoring is realized by calculating the phase difference of the monitoring values of voltage and current at both ends of the cable [13]. However, it is difficult to obtain the voltage signals from the cable joint without affecting normal operation. If the voltage cannot be monitored, only the trend of the change of the three-phase dielectric loss would be obtained.

Currently, there are also some condition analysis methods only based on the sheath current monitoring. The variation of the sheath current is directly analyzed by these methods, but are affected by the operating state of the system [14]. Partial discharge (PD) is another indicator of insulation condition, the discharges of tiny insulation defects are measured to reflect the condition of the insulation. There are two methods of PD measurement, online and offline [15], but no matter which method, the monitoring, reconstruction and location of PD signals are not easy tasks.

Recently, insulation degradation analysis techniques such as Extended Voltage Response [16], [17], [18] and Polarization Depolarization Current [19], [20] have also attracted attention. In [16], the relationship between the material properties and the voltage response measurement has been firstly presented. In [17], the voltage response method has been developed by the systematic changing of the discharging times, which makes the method more precisely. In [18], the extended voltage response method has been used for the aging detection of low-voltage power cables, which shows a conclusive potential. In [19] and [20], the polarization and depolarization currents have been used as aging indicators for cables and show a good correlation. However, these methods are mainly suitable for offline testing and not suitable for online monitoring.

Broadband Impedance Spectroscopy (BIS) technology does not require a high-voltage (HV) power supply and has become a new research trend in recent years. With the method, the input impedance of the cable segment is measured with a sweep signal covering a wide frequency range. The difference between the healthy condition and the aging and/or deterioration condition will be reflected in the impedance spectroscopy. In [21], the Halden Reactor Project developed a method called the Line Resonance Analysis (LIRA) for cable condition monitoring based on BIS. In the project, the cable body and joint are modeled respectively, and different parameters are used in the transmission line model to make the model more applicable. In addition, LIRA uses a smoothing processing model to make the results of each calculation part smoother. The core idea is to process different connection data through the sigmoid function. However, since the sigmoid function contains different types and cannot correspond to the physical meaning, theoretically, the practical application of this technique is limited in terms of parameter matching.

In [22], a kernel function for integral transformation was introduced. After the impedance spectroscopy of the line has been measured at the head end, the impedance spectroscopy is equivalent to a function of frequency and position, and the frequency is integrated to obtain a function that is only related to position. Finally, the local deterioration location is realized using the function. Therefore, the location result of actual aging depends on the choice of the kernel function. Theoretically, no matter which kernel function is chosen, it cannot be applied to all cables, because the electrical parameters are different. Even if the kernel function is customized according to different cables, the solution of the function is not a general solution either.

In [23], a BIS based phase-frequency analysis method for nuclear power plants was developed. The core idea is to compare the difference between the phase-frequency impedance spectroscopy of the healthy cable and the cable under test, then customize the feature extraction algorithm according to the phase-frequency difference, and finally locate the local aging and/or deterioration based on the phase-frequency difference. The diagnostic rules established by this method are suitable for the important and small number of cables in nuclear power plants, but too complicated for the application of grid companies.

In [24], [25], and [26], a method combining frequency domain reflectometry and inverse fast Fourier transform has been proposed, and it can locate the degradation or abnormality in a polymer-insulated cable even if the degradation or abnormality occurs uniformly over the entire cable length. The spatial resolution of the method has been further examined by heating an LDPE-insulated coaxial cable locally as a substitute measure for giving actual degradation to the cable.

Inspired by the above researches, this paper further studies the influence of different load rates under on-line condition, the decoupling problem between the three-phase conductors and the effect of local aging and/or deterioration size. The influence of these factors on the impedance spectroscopy has been comprehensively analyzed. Finally, a whole set of possible diagnostic procedures and criteria are proposed. The proposed method can diagnose four categories of MV cable state: ''healthy,'' ''overall aging,'' ''large-size deterioration'' and ''small-size deterioration,'' and gives the possible extent of aging, deterioration size and location.

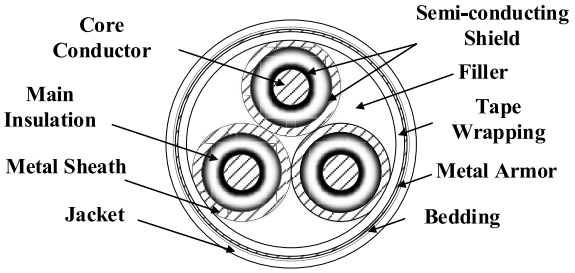

FIGURE 1. Cross-section of a typical MV cable.

II. IMPEDANCE SPECTROSCOPY OF MV CABLES

A. TYPICAL STRUCTURE ANALYSIS OF MV CABLES

A typical MV cable has a three-core structure, and its cross-section is shown in Figure 1. Compared with single-core cables, the cross-sectional structure of three-core cable is more complex, and the number of metal layers is relatively larger.

For the three-core cable presented in Figure 1, the distance between the three-phase conductors is relatively close, and the electromagnetic coupling effect cannot be ignored. Since the geometrical positions of the three-phase conductors are symmetrical, and the metal sheaths share the same ground, the one-phase working capacitance per unit length C_p of the three-core cable is the sum of the self-partial capacitance per unit length C_{kk} and the mutual partial capacitance per unit length C_{ij}. The expression of C_p of can be presented in (1). The subscripts k, i, j represent the serial numbers of the three-phase conductors, $k, i, j \in \{1, 2, 3\}$.

$$C_p = C_{kk} + 3C_{ij} \tag{1}$$

The self-partial capacitance per unit length C_{kk} is only related to the single-phase structure, and its expression is shown in (2).

$$C_{kk} = \frac{2\pi\varepsilon_1}{\ln\frac{r_2}{r_1}} \tag{2}$$

In (2), ε_1 is the dielectric constant of the main insulation, r_1 is the radius of the core conductor, r_2 is the outer radius of the main insulation.

The mutual partial capacitance per unit length C_{ij} is related to the geometric size and relative position of the conductors, and its expression is shown in (3).

$$C_{ij} = \frac{\pi\varepsilon_{\mathrm{Fi}}}{\ln\frac{d-(r_1+b)}{r_1-b}} \tag{3}$$

In (3), $\varepsilon_{\mathrm{Fi}}$ is the dielectric constant of the filler, whose value is close to the dielectric constant of vacuum ε_0; d is the distance between the conductors, b is the distance between the electrical shaft and the conductor's center. The expression of b can be shown in (4).

$$b = \frac{d}{2} - \sqrt{\left(\frac{d}{2}\right)^2 - r_1^2} \tag{4}$$

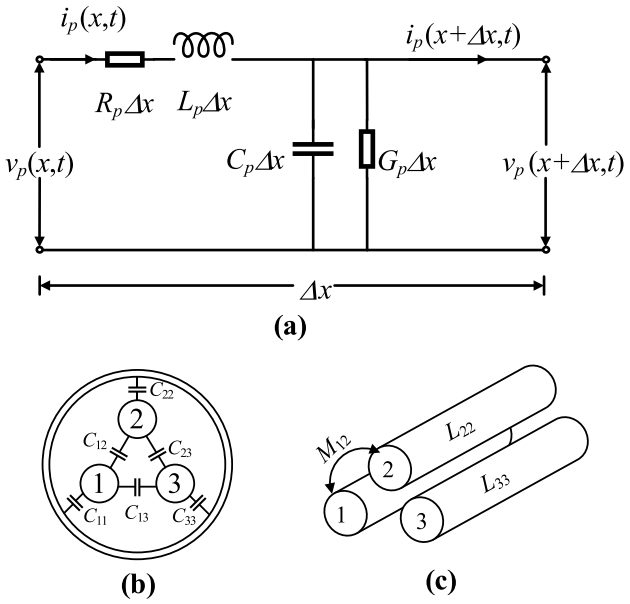

FIGURE 2. Schematic diagram of the impedance parameters of the three-core cable. The interrelationships between the impedance parameters are as follows: (a) equivalent circuit parameters of one-phase cable per unit length; (b) schematic diagram of equivalent circuit of partial capacitance of the three-core cable; (c) schematic diagram of the inductance parameters.

On the other hand, the one-phase inductance of a three-core cable is the sum of its self-inductance and mutual inductance. The expression of the self-inductance per unit length L_{kk} can be shown in (5).

$$L_{kk} = \frac{\mu}{8\pi} \tag{5}$$

In (5), μ is the magnetic permeability of the core conductor.

The mutual inductance M_{ij} between two parallel conductors with the length l and the distance d can be presented in (6).

$$M_{ij} = \frac{\mu l}{2\pi}\left(\ln\left(\frac{l}{d} + \sqrt{1+\frac{l^2}{d^2}}\right) - \sqrt{1+\frac{d^2}{l^2}} + \frac{d}{l}\right) \tag{6}$$

If $d \ll l$, a simpler approximate formula can be obtained through Taylor's expansion as shown in (7).

$$M_{ij} = \frac{\mu l}{2\pi}\left(\ln\left(\frac{2l}{d}\right) - 1\right) \tag{7}$$

The interrelationships between the impedance parameters are shown in Figure 2. Figure 2(a) presents the axial circuit parameters of one-phase, Figures 2(b) and 2(c) present the radial capacitance and inductance parameters of the three-phase cable, respectively. In the figure, Δx represents the unit length, t represents time, C_{11}, C_{22}, C_{33} represent the self-partial capacitance per unit length of Core Conductor 1, 2, 3, respectively, C_{12} represents the mutual partial capacitance per unit length between Core Conductor 1 and Core Conductor 2, C_{13} represents the mutual partial capacitance per

unit length between Core Conductor 1 and Core Conductor 3, C_{23} represents the mutual partial capacitance per unit length between Core Conductor 2 and Core Conductor 3; L_{11}, L_{22}, L_{33} represent the self-inductance per unit length of Core Conductor 1, 2, 3, respectively, M_{12} represents the mutual inductance per unit length between Core Conductor 1 and Core Conductor 2, M_{13} represents the mutual inductance per unit length between Core Conductor 1 and Core Conductor 3, M_{23} represents the mutual inductance per unit length between Core Conductor 2 and Core Conductor 3. The axial parameters are mainly determined by the transmission line model [24], which will be further elaborated in section II-B. When the geometric positions of the three-phase cores of the cable are symmetrical and the material parameters are consistent, the self-partial capacitance per unit length $C_{kk} = C_{11} = C_{22} = C_{33}$, the mutual partial capacitance per unit length $C_{ij} = C_{12} = C_{13} = C_{23}$, the self-inductance per unit length $L_{kk} = L_{11} = L_{22} = L_{33}$, the mutual inductance $M_{ij} = M_{12} = M_{13} = M_{23}$.

B. TRANSMISSION LINE MODEL OF MV CABLES

In this paper, the transmission line equation [24] is chosen to describe the relationship between the voltage, current and electrical distance of the power transmission line. For transmission lines with multi-layer metal structures, such as three-core cables, the electrical parameters in the transmission line equation are vector matrices, as shown in (8).

$$\begin{cases} \dfrac{d\boldsymbol{V}}{dx} = -\boldsymbol{Z}\cdot\boldsymbol{I} \\ \dfrac{d\boldsymbol{I}}{dx} = -\boldsymbol{Y}\cdot\boldsymbol{V} \end{cases} \tag{8}$$

In (8), $\boldsymbol{V}$ and $\boldsymbol{I}$ represent the n-dimensional voltage and current vectors of the n-layer metal structure transmission line at electrical distance x, respectively, $\boldsymbol{Z}$ and $\boldsymbol{Y}$ represent the n-dimensional impedance and admittance matrix, respectively, and n represents the number of radial metal structures on the transmission line. For the three-core structure shown in Figure 1, there are 7 layers of metal structure, therefore, $n = 7$.

For convenience and consistency with the description of the actual single-phase measurement, the subsequent equations are in single-phase form. Thus, the 2nd order partial derivative of the transmission line equation is formed as shown in (9).

$$\begin{cases} \dfrac{d^2V_p(x)}{dx^2} = \left(R_p + j\omega L_p\right)\left(G_p + j\omega C_p\right)V_p(x) \\ \dfrac{d^2I_p(x)}{dx^2} = \left(R_p + j\omega L_p\right)\left(G_p + j\omega C_p\right)I_p(x) \end{cases} \tag{9}$$

In (9), $V_p(x)$ is the single-phase voltage of the cable at the distance of x, $I_p(x)$ is the single-phase current of the cable at the distance of x, R_p is the single-phase resistance per unit length of the cable, L_p is the single-phase inductance per unit length of the cable, G_p is the single-phase conductance per unit length of the cable, C_p is the single-phase capacitance per unit length of the cable. The general solution of (9) can be presented in (10).

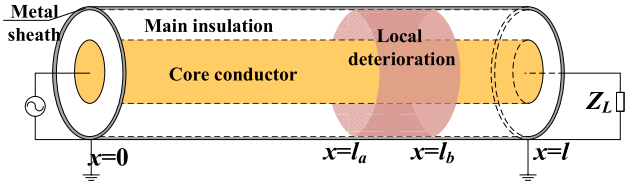

FIGURE 3. Schematic diagram of local deterioration of single-phase cable and its measurement, l_a represents the starting point of local deterioration, l_b represents the end point of local deterioration.

$$\begin{cases} V_p(x) = V_p^+ e^{-\gamma_p x} + V_p^- e^{\gamma_p x} \\ I_p(x) = \dfrac{V_p^+ e^{-\gamma_p x} - V_p^- e^{\gamma_p x}}{Z_{p0}} \end{cases} \tag{10}$$

In (10), V_p^+ and V_p^- represent the forward voltage wave and reflected voltage wave, respectively, and need to be determined by boundary conditions; γ_p and Z_{p0} represent the single-phase propagation coefficient and characteristic impedance of the cable, respectively, which can be shown in (11) and (12).

$$\gamma_p = \sqrt{\left(R_p + j\omega L_p\right)\left(G_p + j\omega C_p\right)} \tag{11}$$

$$Z_{p0} = \sqrt{\frac{R_p + j\omega L_p}{G_p + j\omega C_p}} \tag{12}$$

C. IMPEDANCE SPECTROSCOPY

The impedance spectroscopy of three-core MV cable can be expressed in (13).

$$Z_p(x) = \frac{V_p(x)}{I_p(x)} = Z_{p0}\frac{1 + \Gamma_p e^{2\gamma_p(x-l)}}{1 - \Gamma_p e^{2\gamma_p(x-l)}} \tag{13}$$

In (13), $Z_p(x)$ is the single-phase impedance of the cable at the distance x, Γ_p is the single-phase load reflection coefficient, which can be presented in (14).

$$\Gamma_p = \frac{Z_L - Z_{p0}}{Z_L + Z_{p0}} \tag{14}$$

In (14), Z_L is the load of the transmission line. If the line is open-circuited, Z_L approaches infinity, and Γ_L is 1.00. If the line is short-circuited, Z_L approaches 0, and Γ_L is -1.00.

For convenience of presentation, a schematic diagram of single-phase cable impedance spectroscopy monitoring has been presented in Figure 3. Generally, the measurement position is selected at the head end, that is, the position where $x = 0$ in the figure. Thus, the transmission parameters of the

single-phase cable can be shown in (15) – (18).

$$R_p = R_{cp} + \frac{1}{3}R_{sp} = \frac{\rho_c}{\pi r_1^2} + \frac{\rho_s}{3\pi\left(r_3^2 - r_2^2\right)} \tag{15}$$

$$\begin{aligned} L_p &= L_{kk} + L_s + M_{cs} + \frac{2M_{ij}}{l} \\ &= \frac{\mu}{8\pi} + \frac{\mu}{2\pi}\left(\frac{\left(r_3^2 - 3r_2^2\right)}{4\left(r_3^2 - r_2^2\right)} + \frac{r_2^4 \ln\left(r_3/r_2\right)}{4\left(r_3^2 - r_2^2\right)}\right. \\ &\quad \left. + \ln\left(\frac{r_3}{r_2}\right)\right) + \frac{\mu}{\pi}\left(\ln\left(\frac{2l}{d}\right) - 1\right) \end{aligned} \tag{16}$$

$$G_p + j\omega C_p = j\omega\left(\frac{2\pi\varepsilon_1}{\ln\left(\frac{r_2}{r_1}\right)} + \frac{3\pi\varepsilon_0}{\ln\frac{d-(r_1+b)}{r_1-b}}\right) \tag{17}$$

$$\varepsilon_1 = \frac{A\varepsilon_0}{1 + B\left(j\omega\right)^p} \tag{18}$$

In (15), R_{cp} is the single-phase resistance of the core conductor, R_{sp} is the single-phase resistance of the metal sheath, r_3 is the outer radius of the metal sheath, ρ_c and ρ_s are the conductivity of the core conductor and the metal sheath, respectively. It is to be noted that the skin effect is neglected for the multi-conductor stranded structure of the core conductor and the hollow-circle structure for the metal sheath. In (16), L_s is the self-inductance of the metal sheath, M_{cs} is the mutual inductance between the core conductor and the metal sheath. In (18), A and B are fitting constants, and p is a parameter in the range of 0-1; the expression can be taken as a simplification based on the Cole-Cole model [28].

D. DETERMINATION OF AGING AND LOCAL DETERIORATION

The aging stressor of the main insulation considered in the paper is mainly thermal stress. Thus, the dielectric constant/permittivity can be used as the aging indicator. The permittivity can be expressed in complex form, i.e., with real and imaginary parts. The real part corresponds to the capacitive effect of the insulation, while the imaginary part represents the conductance effect of the insulation. The ratio of the imaginary part to the real part of the dielectric constant is defined as the dielectric loss tangent, tan δ, also known as the loss factor. It is generally believed that the larger the tan δ value, the higher the aging degree.

For the local deterioration as shown in Figure 3, the position and the size of the deterioration can be defined by the distances, l_a and l_b. Thus, the single-phase cable can be divided into three segments. The permittivity of the deterioration is defined as ε_d. Then the impedance spectroscopy of the single-phase cable with local deterioration can be calculated segment by segment. Firstly, the impedance Z_b at position $x = l_b$ can be directly calculated by (13). Secondly, the impedance Z_a at position $x = l_a$ can be calculated by taking Z_b as the load. Finally, the impedance at position $x = 0$ can be calculated by (19).

TABLE 1. Basic structural and material parameters of the object cable.

The structural Parameters	Value (mm)
r_1	11.9
r_2	17.2
r_3	18.2
The Material Parameters	Value (Ω·m)
ρ_c	1.68×10^{-8}
ρ_s	1.68×10^{-8}

TABLE 2. Geometric parameters for YJV22-8.7/15-3*400 type cable.

Serial number	Structure	Material	Radius/Thickness (mm)
1	Core Conductor	Copper	11.9
2	Conductor Shield	Polyolefin	0.4
3	Main Insulation	XLPE	4.5
4	Insulation Shield	Polyolefin	0.4
5	Metal Sheath	Copper	0.2
6	Filler	Polypropylene Mesh Fiber	39.4
7	Tape Wrapping	Polyvinyl Chloride	2
8	Metal Armor	Steel	0.8
9	Jacket	Polyvinyl Chloride	4

$$\begin{cases} Z_b = Z_{0h}\dfrac{1 + \Gamma_1 e^{2\gamma_h(l_b - l)}}{1 - \Gamma_1 e^{2\gamma_h(l_b - l)}} \\ Z_a = Z_{0d}\dfrac{1 + \Gamma_2 e^{2\gamma_d(l_a - l_b)}}{1 - \Gamma_2 e^{2\gamma_d(l_a - l_b)}} \\ Z_{x0} = Z_{0h}\dfrac{1 + \Gamma_3 e^{-2\gamma_h l_a}}{1 - \Gamma_3 e^{-2\gamma_h l_a}} \end{cases} \tag{19}$$

In (19), Z_b, Z_a, and Z_{x0} are, respectively, the impedances at position $x = l_b$, $x = l_a$, and $x = 0$; Z_{0h} and Z_{0d} are the characteristic impedances of the health and degraded segment; γ_h and γ_d are the propagation coefficients of the healthy and degraded segment; and Γ_1, Γ_2, and Γ_3 are the load reflection coefficient of each segment, which can be shown in (20).

$$\begin{cases} \Gamma_1 = \dfrac{Z_L - Z_{0h}}{Z_L + Z_{0h}} \\ \Gamma_2 = \dfrac{Z_b - Z_{0d}}{Z_b + Z_{0d}} \\ \Gamma_3 = \dfrac{Z_a - Z_{0h}}{Z_a + Z_{0h}} \end{cases} \tag{20}$$

III. SIMULATIONS AND RESULTS

A. IMPEDANCE SPECTROSCOPY FOR HEALTHY AND AGED MV CABLES

The cable type YJV22-8.7/15-3*400 [29] is a typical cable structure, which is used for the simulation in the paper. The length of the cable is 20 meters and the other parameters are presented in Table 1, and more detailed cable structural parameters can be found in the Table 2. All simulations in the paper were carried out using MATLAB.

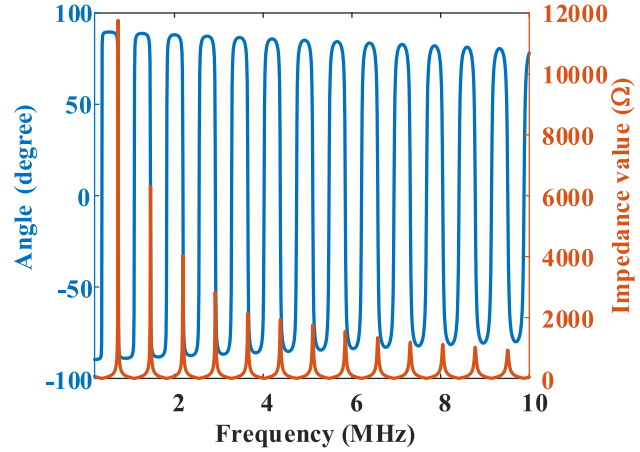

(a) Phase and magnitude spectroscopy

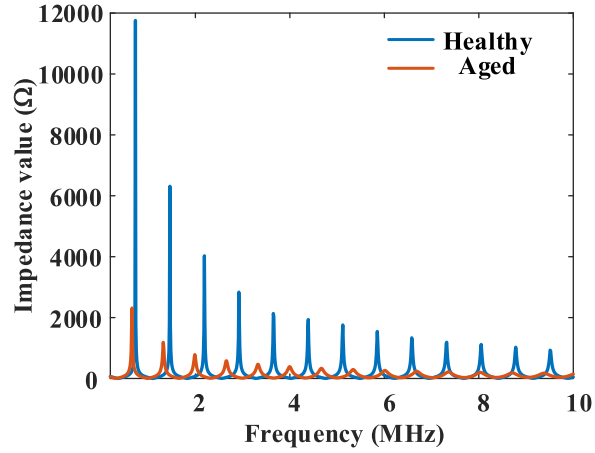

(b) Magnitude spectroscopy of the cable in healthy and aged states

FIGURE 4. Impedance spectroscopy of the cable in healthy and aged states under open-circuit operation. (a) Phase and magnitude spectroscopy of the cable under healthy condition, the line in blue represents the phase angle of the impedance, the line in red represents the magnitude of the impedance. (b) Magnitude spectroscopy of the cable in healthy and aged states.

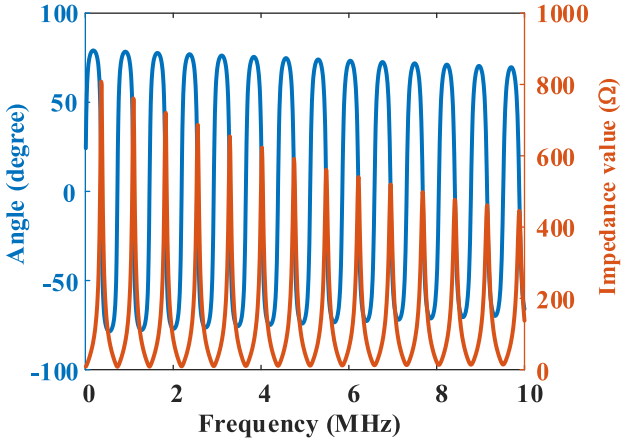

(a) Phase and magnitude spectroscopy

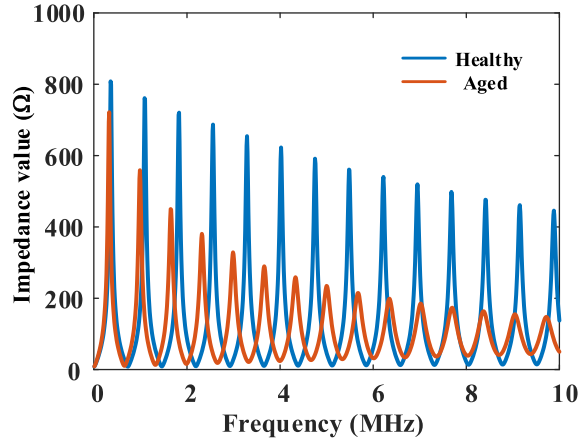

(b) Magnitude spectroscopy of the cable in healthy and aged states.

FIGURE 5. Impedance spectroscopy of the cable in healthy and aged states under full-load operation. (a) Phase and magnitude spectroscopy of the cable under healthy condition, the line in blue represents the phase angle of the impedance, the line in red represents the magnitude of the impedance. (b) Magnitude spectroscopy of the cable in healthy and aged states.

First, the impedance spectroscopy of the cable in healthy and aged states under open-circuit and full-load operation are simulated, respectively. The frequency range is 10 kHz – 10 MHz. The fitting parameters of (18) for the healthy cables are, respectively, $A = 2.68$, $B = 0.14$, and $p = 0.02$. Namely, the relative permittivity is about 2.3, and the value of tan δ is about 4.3×10^{-3}. Meanwhile, the fitting parameters for the aged cables are, respectively, $A = 4.26$, $B = 0.22$, $p = 0.05$, and the relative permittivity is about 3.3, and the value of tan δ is about 0.02. According to (12), the impedance spectroscopy for healthy and aged cables under open-circuit operation at the position of $x = 0$ can be presented in Figure 4.

As shown in Figure 4(a), under open-circuit operation, the impedance phase angle of the one-phase cable is periodic oscillation attenuation with the frequency increases, and the impedance magnitude is periodic pulse attenuation with the increase of frequency. Furthermore, the attenuation of the impedance magnitude is more significant. The periodic impedance pulse is related to the resonance of the overall inductance and capacitance at a certain frequency. In Figure 4(b), affected by the changes in aging states, the magnitude spectroscopy in health and aged state is significantly different.

Similarly, the impedance spectroscopy for healthy and aged cables under full-load operation at the position of $x = 0$ can be presented in Figure 5.

As shown in Figure 5(a), under full-load operation, the impedance phase angle and the impedance magnitude have the similar trend to that under open-circuit operation. In Figure 5(b), the impedance magnitude under full-load operation is lower than that under open-circuit operation, while the trends are still similar. The reason for the impedance resonance peak is the refraction and reflection of the wave process. The reflection coefficient under open-circuit operation is 1, and the reflection coefficient under full-load operation is less than 1. This is also the main reason that impedance

magnitude under full-load operation is lower than that under open-circuit operation.

B. IMPEDANCE SPECTROSCOPY FOR LOCAL DETERIORATION

Due to the complex channel environment of distribution MV cables, a distribution MV cable may pass through a variety of different environments (air, soil, water, etc.), resulting in different degrees of aging in different segments. Segments with harsh environments tend to have local aging and/or deterioration problems. For convenience, the above-mentioned cable model and parameters are used to simulate the impedance magnitude spectroscopy of l_a = 1-19 m when the local deterioration length is 0.1 m, as shown in Figure 6.

As presented in Figure 6, the impedance magnitude spectroscopy in the case of a small local deterioration size is not much different from the healthy state as a whole. It can be seen from the partial enlarged figures of the first and last resonance peaks that the resonance peaks at different local deterioration positions are different, and the difference of the last resonance peak is greater than that of the first resonance peak. Furthermore, as the frequency increases, the difference in resonance peaks also increases.

Similarly, the impedance phase angle spectroscopy for local deterioration cables under full-load operation at the position of $x = 0$ can be presented in Figure 7.

As shown in Figure 7, the impedance phase angle spectroscopy in the case of a small local deterioration size is not much different from the healthy state either. The difference of the impedance phase angle spectroscopies under different deterioration positions is also very small. As the frequency increases, the impedance phase angle values become relatively more spread out. Therefore, taking the impedance phase angle and the resonance peak amplitude together as the criterion of local deterioration helps to improve the diagnosis effect.

C. INFLUENCING FACTORS OF THE IMPEDANCE SPECTROSCOPY

The impedance spectroscopy of the MV three-core cable is affected by some factors, such as the size of the local deterioration, the degree of the aging, the length of the cable, etc. The analysis will be carried out separately below.

1) THE SIZE OF THE LOCAL DETERIORATION

Firstly, the size of local deterioration is taken as the single variable, the local deterioration position is fixed at $l_a = 7$ m, and the impedance spectroscopy simulation has been carried out with the sizes of 2, 4, 6, 8, and 10 m, respectively. The impedance spectroscopy can be presented in Figure 8.

Affected by the larger local deterioration sizes, the impedance spectroscopy curves of the cable have some "jumping" change rules, as shown in Figure 8. The resonance peaks are no longer monotonically decreasing with the increase of frequency, as shown in Figure 8(a); the phase angles are not the law of monotonic oscillation attenuation, as shown in Figure 8(b).

TABLE 3. Parameters of the degree of aging.

Serial Number	ε Parameters	Relative Permittivity	Tan δ
1	$A = 2.68$, $B = 0.140$, $p = 0.020$	2.28	0.0047
2	$A = 3.35$, $B = 0.154$, $p = 0.032$	2.75	0.0090
3	$A = 4.02$, $B = 0.168$, $p = 0.044$	3.16	0.0148
4	$A = 4.69$, $B = 0.182$, $p = 0.056$	3.51	0.0222
5	$A = 5.36$, $B = 0.196$, $p = 0.068$	3.79	0.0313
6	$A = 6.03$, $B = 0.210$, $p = 0.080$	4.00	0.0423
7	$A = 6.70$, $B = 0.224$, $p = 0.092$	4.14	0.0553
8	$A = 7.37$, $B = 0.238$, $p = 0.104$	4.18	0.0702
9	$A = 8.04$, $B = 0.252$, $p = 0.116$	4.22	0.0869
10	$A = 8.71$, $B = 0.266$, $p = 0.128$	4.23	0.1055

2) THE DEGREE OF THE AGING

Secondly, the degree of the aging is taken as the single variable, and the main focus here is on the impedance spectroscopy under the overall aging state of the cable. As mentioned before, the dielectric constant/permittivity and the value of tan δ can be used as the indicator of the aging. The simulations are carried out with different parameters of tan δ and the dielectric constant/permittivity as shown in Table 3, and the impedance spectroscopy is presented in Figure 9.

It is to be noted that the parameters in Table 3 are slightly exaggerated to show the effect of aging more comprehensively. In the simulations, the ε parameters shown in Table 3 have been used for the setting. Although the relative permittivity in column 3 and the tan δ value in column 4 can be calculated directly by setting the ε parameters, they cannot directly control the real and imaginary parts of the permittivity.

In Figure 9, with the increase of the aging degree, the impedance magnitude decreases, the amplitude of the resonance peak decreases and the position shifts; the phase in the impedance phase spectroscopy shifts, and the trend of oscillation attenuation becomes more obvious.

3) THE LENGTH OF THE CABLE

Since the impedance spectroscopy is a manifestation of the wave process, it is closely related to the length of the cable. Theoretically, the wave velocity v_p of the cable can be presented in (21), and it is a parameter related only to the structure and material of the cable itself. Then the wavelength λ_p

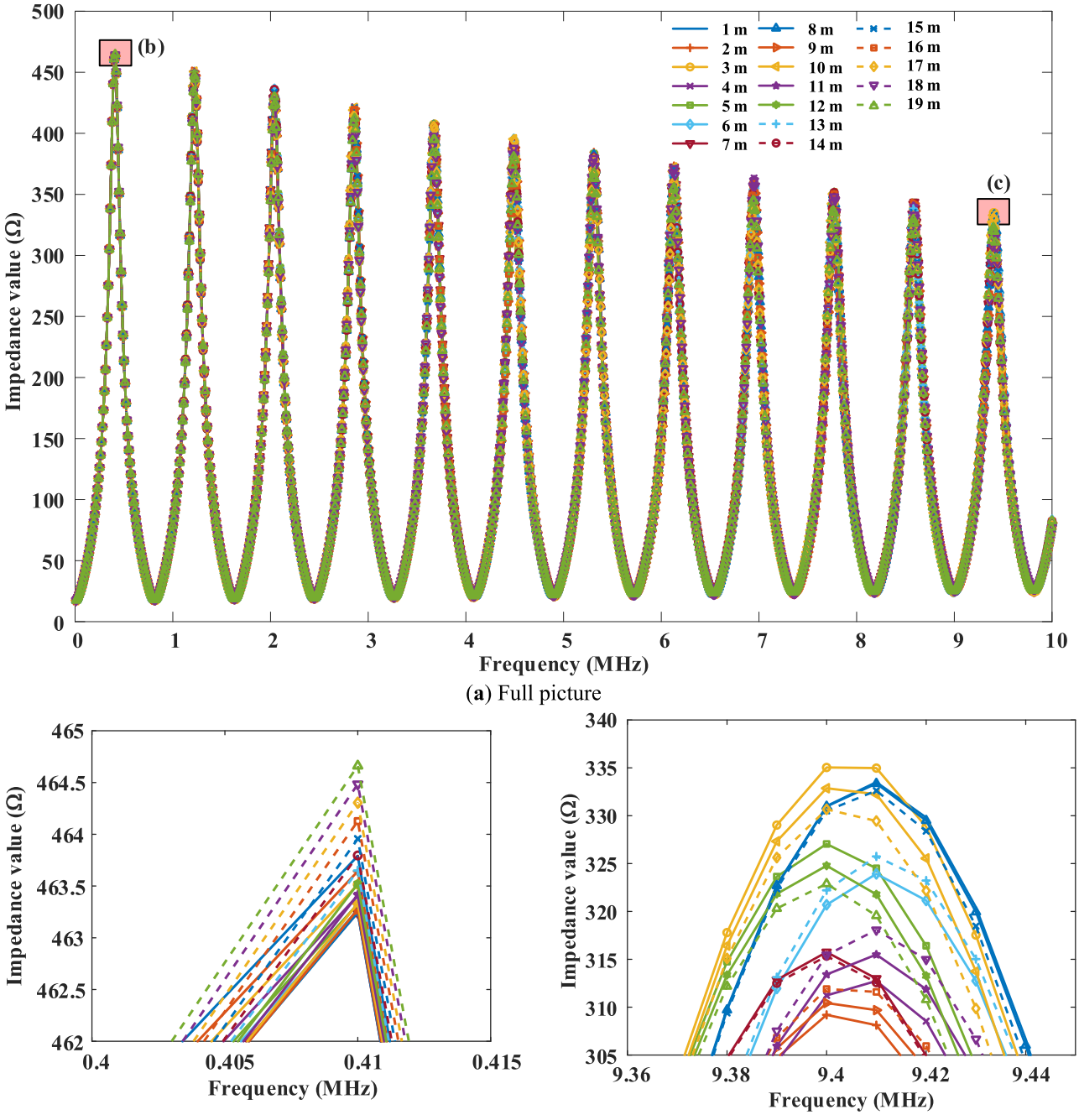

FIGURE 6. Impedance magnitude spectroscopy of the cable with local deterioration under full-load operation. (a) Full figure; (b) Partial figure of the first resonance peak; (c) Partial figure of the last resonance peak.

at the frequency f_p can be shown in (22).

$$v_p = \frac{1}{\sqrt{L_p C_p}} \tag{21}$$

$$\lambda_p = \frac{v_p}{f_p} \tag{22}$$

In reality, for a certain cable, its length l and wave velocity v_p are fixed values in the healthy state. Thus, there is a fixed frequency for the cable in healthy state, which has been defined as the eigen propagation frequency f_{ep}, as presented in (23).

$$f_{ep} \doteq \frac{1}{2l\sqrt{L_p C_p}} \tag{23}$$

It is to be noticed that f_{ep} is the interval between resonant peaks in the impedance magnitude spectroscopy and is also the period of oscillation in the phase spectroscopy. Therefore,

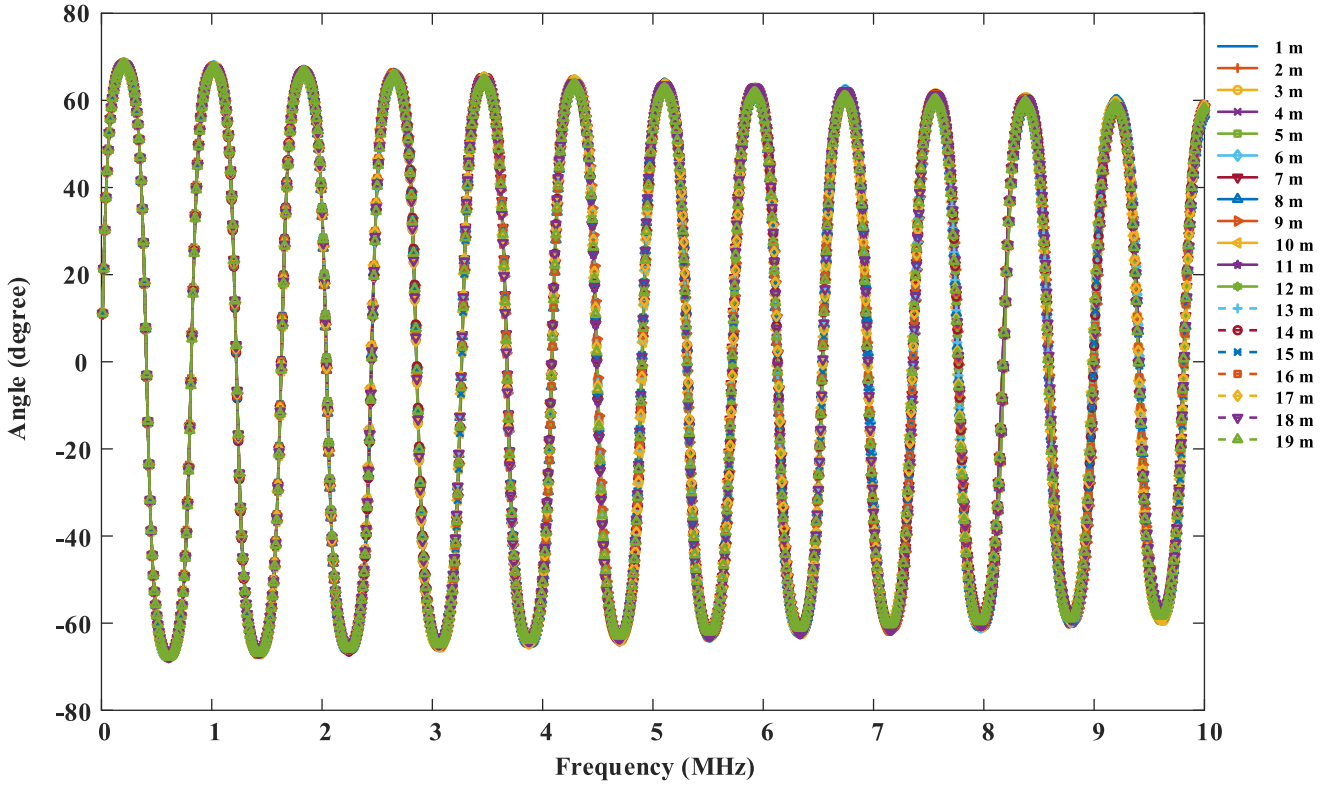

FIGURE 7. Impedance phase angle spectroscopy of the cable with local deterioration under full-load operation.

the length of the cable determines its eigen propagation frequency and further determines the resonant peak interval in its impedance magnitude spectroscopy and the oscillation period in its phase spectroscopy. Thus, the influence of cable length on impedance spectroscopy is most difficult to reflect in the diagnosis of local deterioration of small size, which will be the main research content of this section.

Figures 6 and 7 are the impedance spectroscopy results with the small size local deterioration. Under the situation, the differences of the eigen propagation frequencies are very small. If the length of the cable is taken as the single variable, although the difference in cable length can be judged by the eigen propagation frequency, it is not easy to directly locate the local deterioration.

4) THE LOAD RATE OF THE CABLE

Finally, the load rate of local deterioration is taken as the single variable, which varies from 10% to 100%. The main focus here is on the impedance spectroscopy under the overall aging state of the cable, which can be presented in Figure 10.

As shown in Figure 10, as the loading rate increases, the impedance magnitude spectroscopy becomes steeper, and the amplitude of the resonance peak becomes larger. In other words, the load rate mainly affects the amplitude of the impedance magnitude spectroscopy, and the resonance peak amplitude can be used as the criterion index.

IV. DIAGNOSIS OF THE AGING AND DETERIORATION

In general, for a certain cable in operation, its length and load are known quantities. Therefore, the cable impedance spectroscopy with known length and load rate in healthy state can be directly calculated or tested, and it can be used as a diagnostic benchmark for the aging and/or deterioration. The procedure of the diagnosis of the aging and deterioration can be presented in Figure 11.

As shown in Figure 11, the first step for the diagnosis is to calculate/measure the impedance spectroscopy of the healthy cable and obtain the eigen propagation frequency f_{ep0}. Then, the second step is to measure the impedance spectroscopy of the cable need to be tested and obtain the eigen propagation frequency f_{ep1}. After that, it is necessary to compare whether the monotonous decreasing trend of the resonance peak in the impedance magnitude spectroscopy is consistent with the healthy cable. If the trend is not consistent, it can be determined that the cable is with large-size local deterioration. If the trend is consistent, next is to compare whether the phase angle oscillation amplitude decrease monotonically. If the phase angle oscillation amplitude decreases monotonically, it can be determined that the cable is under overall aging state. After that, the extent of aging can be diagnosed by the impedance resonance peak amplitude. If the amplitude of the phase angle has no obvious monotonically decreasing trend, next is to compare whether the difference between f_{ep0} and f_{ep1} less than the calculation bias. If the difference is

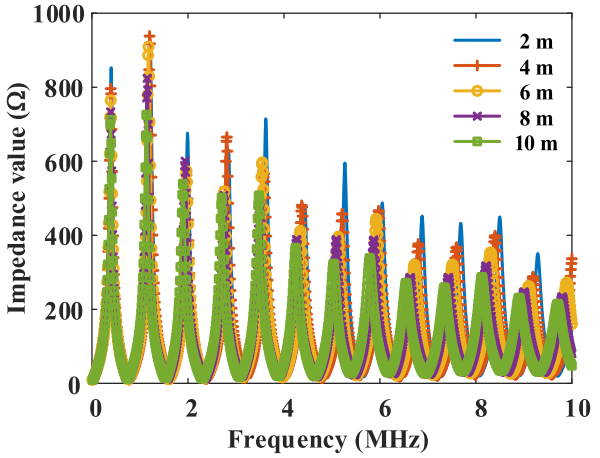

(a) Impedance magnitude spectroscopy

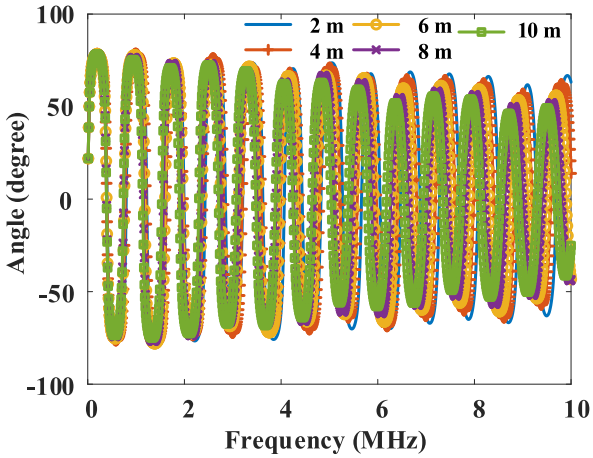

(b) Impedance phase angle spectroscopy.

FIGURE 8. Impedance spectroscopy of the cable with local deterioration of different sizes under full-load operation. (a) Impedance magnitude spectroscopy; (b) Impedance phase angle spectroscopy.

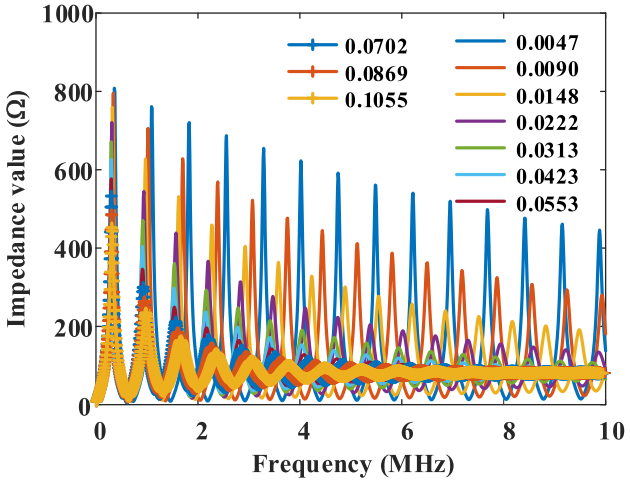

(a) Impedance magnitude spectroscopy

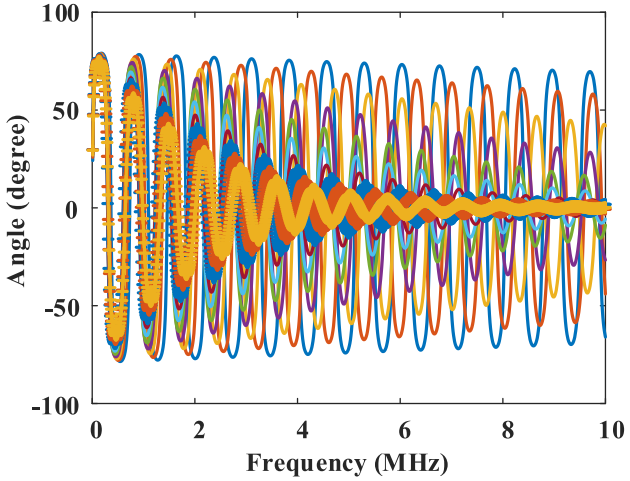

(b) Impedance phase angle spectroscopy.

FIGURE 9. Impedance spectroscopy of the cable in overall aging state under full-load operation with the tan δ value varies from 0.0047 to 0.1055. In the legend, the numbers represent the value of each tan δ, and Figure (a) and (b) share the same legend. (a) Impedance magnitude spectroscopy; (b) Impedance phase angle spectroscopy.

larger than the calculation bias, it can be determined that the cable is with small-size local deterioration. After the local deterioration is determined, next step is to locate the local deterioration. If the difference is less than the calculation bias, it can be determined that the cable is health.

Specifically, the criterion for the trend of the resonance peak can be whether the amplitude of the resonance peak decreases monotonically. Only in the case of local deterioration with larger size, the resonant peaks do not decrease monotonically, as shown in Figure 8. If the frequency of the resonant peak between 8 MHz and 9 MHz in the impedance spectroscopy is used as the characteristic frequency of size criterion, the relationship curve between the characteristic frequency and the deterioration size under the deterioration size of 1 to 10 m can be recalculated, as shown in Figure 12.

As shown in Figure 12, the relationship between the size of the deterioration and the characteristic frequency is monotonous, which is a good characteristic for the criterion. In order to verify the effects for the position and the extent of the local deterioration, the characteristic frequency of the size criterion has been further simulated under different local deterioration positions and degradation degrees, as presented in Figure 13.

As shown in Figure 13, the location of the local deterioration (l_a) has a small effect on the characteristic frequency of size criterion. The impact of the degree of deterioration on the characteristic frequency is mainly reflected in the value, and it has no effect on the trend of the relationship curves. In addition, in the case of large-size deterioration, the discrimination of the first resonance peak impedance value is relatively large, which can be used as the criterion for the position and the size of the deterioration. In order to further propose the criterion of the deterioration position, the relationship between the first resonance peak impedance value and the position of the deterioration has been further calculated, and the results can be presented in Figure 14.

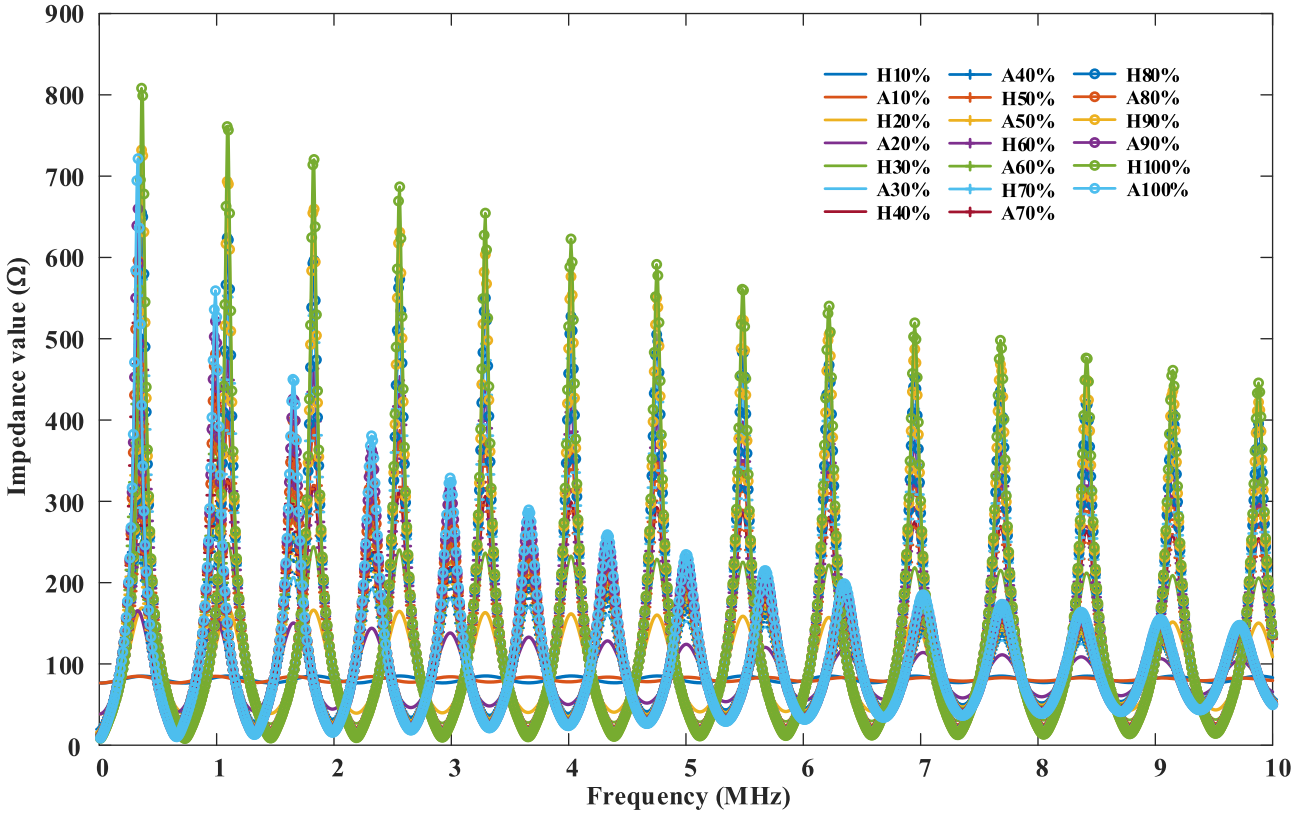

FIGURE 10. Impedance spectroscopy of the cable in healthy and aged states with the load rate varies from 10% to 100%. In the legend, the first letter H represents the healthy state and A represents the aging state.

In Figure 14(a), at the same deterioration position, the larger the size of the degradation, the greater the amplitude of the first resonance peak in the impedance spectroscopy. Therefore, the value of the first resonance peak could be an auxiliary criterion for the position of the deterioration. Similarly, in Figure 14(b), with the increase of the aging, the amplitude of the impedance resonance peak decreases; and as the position of the deterioration l_a increases, the amplitude of the decrease of the resonant peak value also decreases.

The characteristics of the overall aging are relatively obvious, as presented in Figure 9. As the extent of aging increases, the resonant peak value of the impedance magnitude spectroscopy is reduced, and the amplitude in the phase spectroscopy decreases, and gradually tends to zero. After the overall aging is determined, the value of the first resonance peak can be used to determine the specific extent of aging, as shown in Figure 14.

As shown in Figure 15, in the case of overall aging, the first resonance peak value decreases monotonous with the extent of aging. Therefore, it can be a criterion for the overall aging.

The impedance spectroscopies of the small-size deterioration are relatively similar, as shown in Figure 6. The main reason is that the impedance spectroscopy is not sensitive to the position of the deterioration when the size of the deterioration is small. However, it is significantly different from the impedance spectroscopy in a healthy state, which can be determined by the frequency difference between the resonance peaks, i.e., the difference between f_{eq0} and f_{eq1}. It is also can be identified by counting the number of the resonance peaks, as presented in Figures 5 and 6. Both of the frequency ranges are from 10 kHz to 10 MHz, the resonance peak number in Figure 5 (Healthy state) is 14 and the number in Figure 6 is 12. After the small-size deterioration is determined, the most important thing is to locate the position of the deterioration. This work can be accomplished by the comparison of the amplitude and phase angle of the first resonance peak, as presented in Figure 16.

In Figure 16, the phase angle of the first resonance peak has a monotonically increasing relationship with the position of the deterioration, which can be used as the criterion. However, the numerical distribution range of the phase angle is relatively narrow, and the requirements for detection accuracy are relatively high. Therefore, the amplitude of the resonance peak can be used as an auxiliary criterion.

V. DISCUSSION

The feasibility of online diagnosis of aging and local deterioration for MV three-core cables based on impedance spectroscopy has been studied in the paper. A whole set of possible diagnostic procedures and criteria are proposed. However, the selection of the frequency range and the specific criterion for the diagnosis remain to be further studied and discussed.

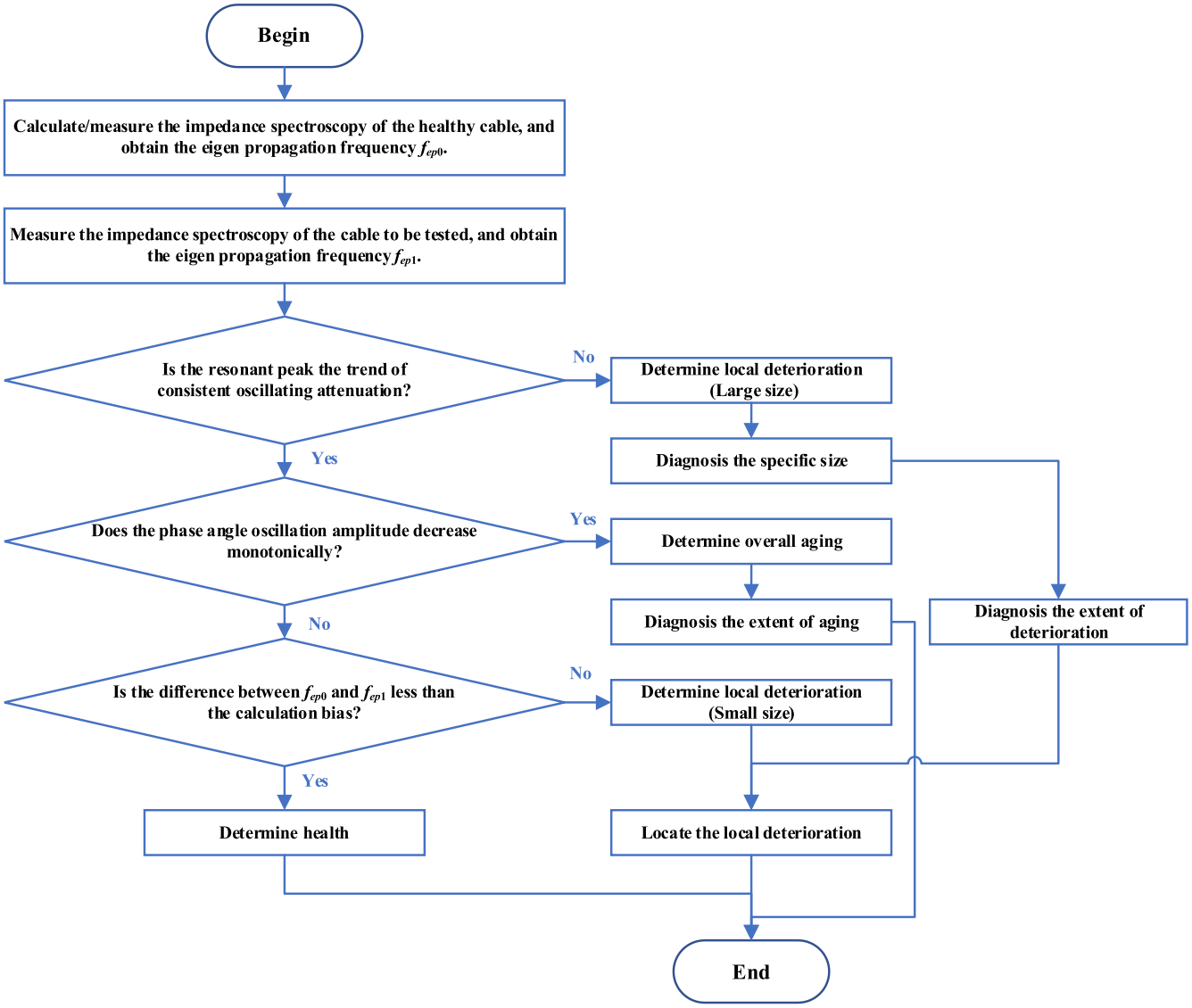

FIGURE 11. Schematic diagram of the procedure of the diagnosis of the aging and deterioration.

A. SELECTION OF THE FREQUENCY RANGE

As presented in (23), the eigen propagation frequency f_{ep} is directly related to the cable length, which means the cables with different lengths should be suitable for different frequency ranges. It is to be noted that the interval between the resonance peaks of the impedance spectroscopy is approximately equal to the eigen propagation frequency. Therefore, in any case, the upper limit of the frequency range of the impedance spectroscopy should be greater than the eigen propagation frequency, so as to ensure that the measured impedance spectroscopy contains at least a resonance peak. However, for the accurate diagnosis, only one resonance peak is far from enough. Based on the situation in the case of the paper, the recommended number of resonance peaks is 10 to 12, that is, the upper limit of the frequency range is 10 to 12 times the eigen propagation frequency. The diagnostic capabilities of different frequency ranges can be summarized in Table 4.

If limited by actual conditions, the highest frequency upper limit can only reach or be slightly greater than f_{ep}, the specific criterion index for the diagnosis only have Z_{pp1} and f_{c1}. In this case, only when the value of the resonance peak and the corresponding frequency have a significant shift, it can be diagnosed as overall aging or large-size deterioration. If the frequency upper limit can reach 4 to 6 times f_{ep}, the diagnosis indicators increase Z_{ppk}, f_{ck}, and local trends in resonance peaks. Thus, overall aging and large-size deterioration could be diagnosed with a high probability, for the high probability of continuous 4 to 6 resonance peaks are enough to reflect its trend. However, small-size deterioration just may be diagnosed with a low probability, the reason is that the discrimination of the impedance spectroscopy is not enough

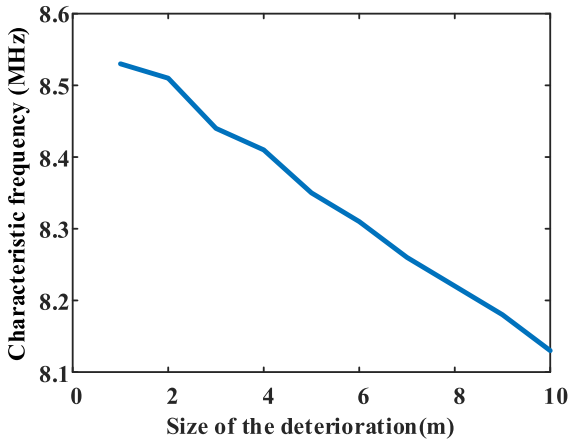

FIGURE 12. Relationship between the size of the deterioration and the characteristic frequency.

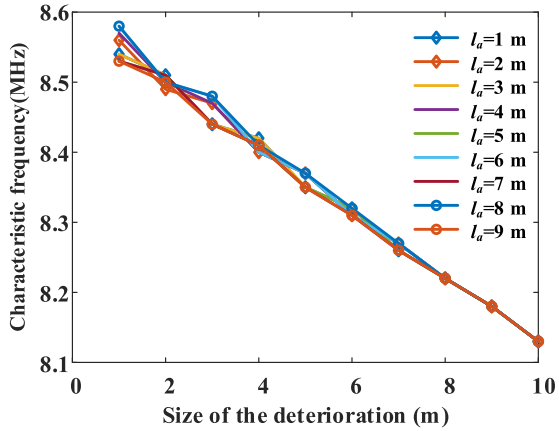

(a) Local deterioration position varies from 1 to 9 meters.

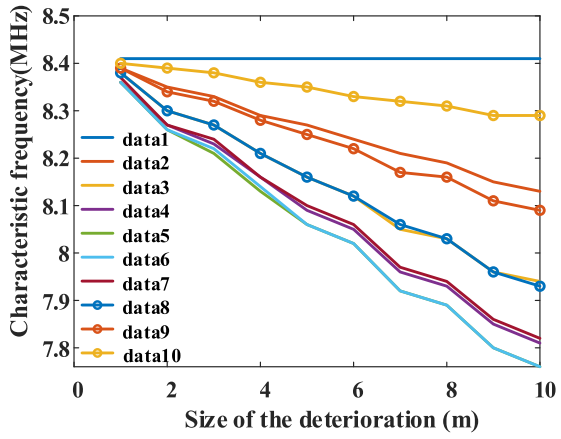

(b) Tan δ value varies from 0.0047 to 0.1055.

FIGURE 13. Relationship between the size of the deterioration and the characteristic frequency under different local deterioration positions and degradation degrees: (a) Local deterioration position varies from 1 to 9 meters; (b) Tan δ value varies from 0.0047 to 0.1055, which are consistent with Table 3.

when the extent of deterioration is slight. Finally, if the frequency upper limit can reach 10 to 12 times f_{ep}, the diagnosis indicators would be relatively complete, and all the overall aging, large-size deterioration and small-size deterioration could be diagnosed.

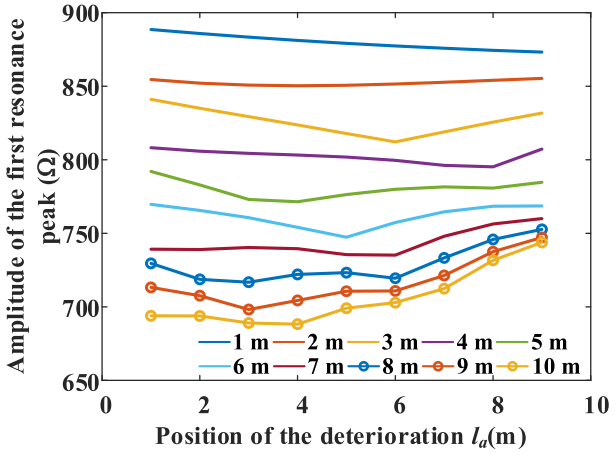

(a) under the size of the deterioration varies from 1 to 10 m

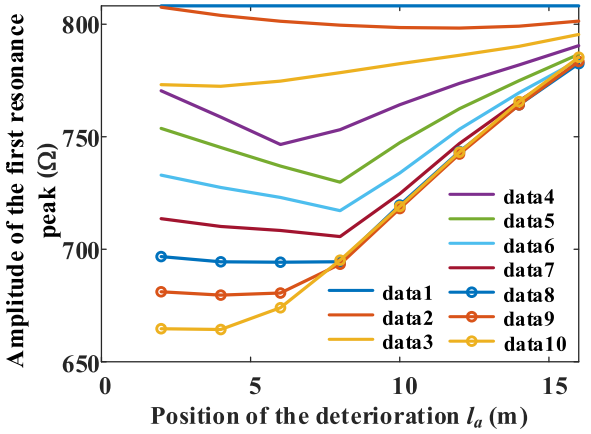

(b) under the tan δ value varies from 0.0047 to 0.1055

FIGURE 14. Relationship between the position of the deterioration and the first resonance peak impedance value: (a) under the size of the deterioration varies from 1 to 10 m; (b) under the tan δ value varies from 0.0047 to 0.1055, which are consistent with Table 3. Z_{pp1} represents the value of the first resonance peak.

TABLE 4. Diagnostic capabilities of different frequency ranges.

The frequency cap	The specific criterion index [a]	The diagnostic capability
f_{ep}	Z_{pp1}, f_{c1}	Whether it is overall aging or large-size deterioration.
4-6 times f_{ep}	$Z_{pp1}, f_{c1}, Z_{ppk}, f_{ck}$, local trends in resonance peaks	Overall aging and large-size deterioration could be diagnosed with a high probability; small-size deterioration may be diagnosed with a low probability
10-12 times f_{ep}	$Z_{pp1}, f_{c1}, Z_{ppk}, f_{ck}$, f_{ep1}, the trends in resonance peaks and phase angles	Overall aging, large-size deterioration and small-size deterioration

[a] Z_{pp1} represents the value of the first resonance peak, f_{c1} represents the frequency of the first resonance peak. Z_{ppk} represents the value of the $k^{\text{-th}}$ resonance peak, f_{ck} represents the frequency of the $k^{\text{-th}}$ resonance peak.

B. SPECIFIC CRITERION FOR THE DIAGNOSIS

The criterion proposed in Section IV is not specific to any hardware devices, and the measurement results of devices

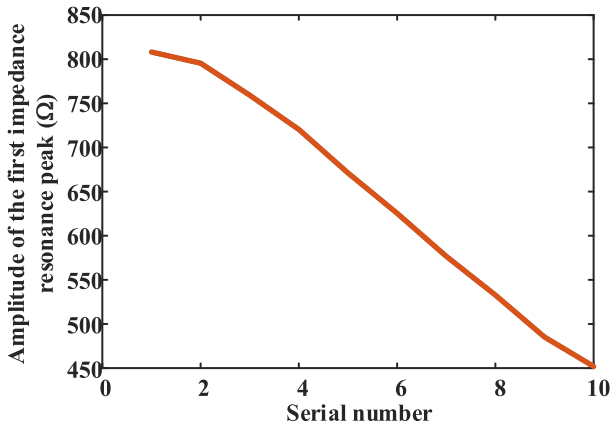

FIGURE 15. Relationship between the value of the first resonance peak and the specific extent of aging. The serial numbers 1 to 10 are consistent with Table 3, which correspond to different relative dielectric constants and tan δ values.

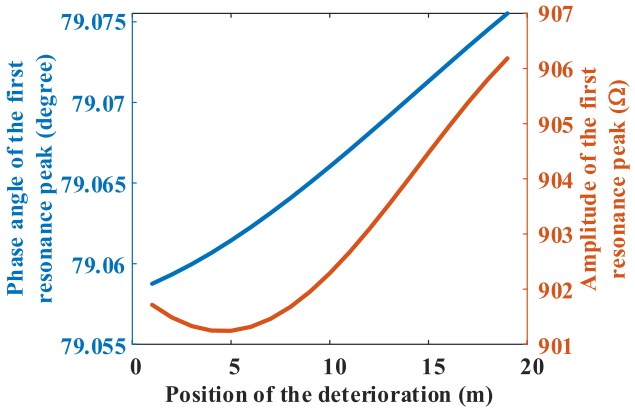

FIGURE 16. Relationship between the position of the deterioration and the amplitude and phase angle of the first resonance peak, under the small-size deterioration state.

with different precisions may have deviations. For the specific hardware device, its actual measurement accuracy should be considered, and the criterion index should be adjusted appropriately. Especially in the case of small-size local deterioration, the requirements for accuracy are relatively high. If the accuracy cannot be achieved, the diagnosis may fail. In addition, the main focus of the paper is medium-voltage three-core cables. The calculation case is just a kind of typical structure, and specific criterion can be deduced for specific cables in engineering applications. However, there are also differences in cable structures and materials. Future research on adaptive algorithm criterion will help reduce the workload.

In addition, since more than 98% of power cables in China use cross-linked polyethylene (XLPE) as the insulating material, the method proposed in the paper has not yet identified and differentiated the insulating material. However, different insulating materials will have differences in impedance parameters, further research will be conducted on the distinction of materials in the future.

VI. CONCLUSION

The feasibility of on-line aging and deterioration diagnosis of medium-voltage three-core cables based on impedance spectroscopy has been studied in the paper, and a set of possible diagnostic procedures and methods have been proposed. The coupling of three-phase conductors can be decoupled phase by phase via comprehensive analysis of multiple conductors. If the load rate can be monitored, the method of impedance spectroscopy can also be used for online monitoring. From the analysis of the impedance spectroscopies of the typical structure of the three-core cable, it can be concluded that:

1) The overall aging can be determined by the monotonous decrease of the value of the resonance peaks and the phase amplitudes, and the extent of aging can be diagnosed by using the value of the first resonance peak. The higher the extent of aging, the smaller value of the first resonance peak.

2) The large-size local deterioration can be determined by the non -monotonous trend of the value of the resonance peaks. The specific size and position of the deterioration can be determined by the characteristic frequency and the value of the first resonance peak.

3) The small-size local deterioration can be determined by the difference between f_{ep0} and f_{ep1}, and the position of the deterioration can be located by using the amplitude and phase angle of the first resonance peak.

REFERENCES

[1] A. A. Hamad and R. A. Ghunem, "A techno-economic framework for replacing aged XLPE cables in the distribution network," *IEEE Trans. Power Del.*, vol. 35, no. 5, pp. 2387–2393, Oct. 2020.

[2] C. Zhou, H. Yi, and X. Dong, "Review of recent research towards power cable life cycle management," *High Voltage*, vol. 2, no. 3, pp. 179–187, Sep. 2017.

[3] Y. Ohki and N. Hirai, "Degradation of flame-retardant cross-linked polyethylene caused by heat, gamma-rays, and steam," *IEEE Access*, vol. 10, pp. 62164–62172, 2022.

[4] T. M. Z. Elsharkawy, G. F. A. Osman, and W. A. A. Salem, "The effect of nonlinear loads on the underground distribution cables: A case study," *J. Electr. Syst. Inf. Technol.*, vol. 9, no. 1, p. 19, Oct. 2022.

[5] A. van Deursen, P. Wouters, and F. Steennis, "Influence of temperature on wave propagation in low-voltage distribution cables," *IEEE Trans. Dielectr. Electr. Insul.*, vol. 28, no. 5, pp. 1785–1792, Oct. 2021.

[6] F. Binot, T. D. Le, and M. Petit, "Characterization and modeling of LV cables considering external parameters for distribution networks," *Energies*, vol. 14, no. 23, p. 7849, Nov. 2021.

[7] N. I. Yermoshin, E. V. Yakimov, A. E. Goldshtein, and D. A. Sednev, "Increase in fast response time of the resistance-to-voltage converter when monitoring the cable products' insulation resistance," *Sensors*, vol. 21, no. 2, p. 368, Jan. 2021.

[8] P. Cheetham, A. Al-Taie, S. Telikapalli, T. Stamm, C. H. Kim, L. Graber, and S. Pamidi, "Development of a high-temperature superconducting gas-insulated power cable," *IEEE Trans. Appl. Supercond.*, vol. 30, no. 6, Sep. 2020, Art. no. 7700207.

[9] T. V. Santhosh, V. Gopika, A. K. Ghosh, B. G. Fernandes, and K. A. Dubey, "Reliability prediction of I&C cable insulation materials by DSC and Weibull theory for probabilistic safety assessment of NPPs," *Nucl. Eng. Design*, vol. 296, pp. 51–61, Jan. 2016.

[10] H. Wang, M. Sun, K. Zhao, X. Wang, Q. Xu, W. Wang, and C. Li, "High-voltage FDS of thermally aged XLPE cable and its correlation with physic-ochemical properties," *Polymers*, vol. 14, no. 17, p. 3519, Aug. 2022.

[11] C. C. Uydur and O. Arikan, "Use of tanδ and partial discharge for evaluating the cable termination assembly," *Energies*, vol. 13, no. 20, p. 5299, Oct. 2020.

[12] S. V. Suraci, C. Li, and D. Fabiani, "Dielectric spectroscopy as a condition monitoring technique for low-voltage cables: Onsite aging assessment and sensitivity analyses," *Energies*, vol. 15, no. 4, p. 1509, Feb. 2022.
[13] Y. Yang, D. M. Hepburn, C. Zhou, W. Zhou, W. Jiang, and Z. Tian, "On-line monitoring and analysis of the dielectric loss in cross-bonded HV cable system," *Electric Power Syst. Res.*, vol. 149, pp. 89–101, Aug. 2017.
[14] C. Zhou, Y. Yang, M. Li, and W. Zhou, "An integrated cable condition diagnosis and fault localization system via sheath current monitoring," in *Proc. Condition Monitor. Diagnosis (CMD)*, Xi'an, China, 2016, pp. 1–8.
[15] Y. Yang, D. M. Hepburn, C. Zhou, W. Zhou, and Y. Bao, "On-line monitoring of relative dielectric losses in cross-bonded cables using sheath currents," *IEEE Trans. Dielectr. Electr. Insul.*, vol. 24, no. 5, pp. 2677–2685, Oct. 2017.
[16] E. Németh, "Proposed fundamental characteristics describing dielectric processes in dielectrics," *Periodica Polytechnica Electr. Eng.*, vol. 15, no. 4, pp. 305–322, 1971.
[17] Z. Á. Tamus, D. Csábi, and G. M. Csányi, "Characterization of dielectric materials by the extension of voltage response method," *J. Phys., Conf.*, vol. 646, Oct. 2015, Art. no. 012043.
[18] E. Mustafa, R. S. A. Afia, and Z. Á. Tamus, "Dielectric loss and extended voltage response measurements for low-voltage power cables used in nuclear power plant: Potential methods for aging detection due to thermal stress," *Electr. Eng.*, vol. 103, no. 2, pp. 899–908, Apr. 2021.
[19] E. Mustafa, R. S. A. Afia, O. Nouini, and Z. Á. Tamus, "Implementation of non-destructive electrical condition monitoring techniques on low-voltage nuclear cables: I. irradiation aging of EPR/CSPE cables," *Energies*, vol. 14, no. 16, p. 5139, Aug. 2021.
[20] E. Mustafa, R. S. A. Afia, A. Nawaz, O. Nouini, and Z. Á. Tamus, "Implementation of non-destructive condition monitoring techniques on low-voltage nuclear cables: II. Thermal aging of EPR/CSPE cables," *Energies*, vol. 15, no. 9, p. 3231, Apr. 2022.
[21] T. Maier, D. Lick, and T. Leibfried, "Frequency-domain cable model with a real representation of joints and smooth failure changes and a diagnostic investigation with line resonance analysis," in *Proc. Condition Monitor. Diagnosis (CMD)*, Sep. 2018, pp. 1–6.
[22] Z. Zhou, D. Zhang, J. He, and M. Li, "Local degradation diagnosis for cable insulation based on broadband impedance spectroscopy," *IEEE Trans. Dielectr. Electr. Insul.*, vol. 22, no. 4, pp. 2097–2107, Aug. 2015.
[23] D. Rogovin and R. Lofaro, "Evaluation of the broadband impedance spectroscopy prognostic/diagnostic technique for electric cables used in nuclear power plants," U.S. Nucl. Regulatory Commission, Washington, DC, USA, Tech. Rep. NUREG/CR-6904, 2005. [Online]. Available: https://www.nrc.gov/reading-rm/doc-collections/nuregs/contract/cr6904/cr6904.pdf
[24] *Electric Cables—Calculation of the Current Rating—Part1-1: Current Rating Equations (100 % Load Factor) and Calculation of Losses—General*, International Electrotechnical Commission, Geneva, Switzerland, document IEC 60287-1-1:2006+A1:2014, 2014.
[25] Y. Ohki and N. Hirai, "Location attempt of a degraded portion in a long polymer-insulated cable," *IEEE Trans. Dielectr. Electr. Insul.*, vol. 25, no. 6, pp. 2461–2466, Dec. 2018.
[26] Y. Ohki and N. Hirai, "Detection of abnormality occurring over the whole cable length by frequency domain reflectometry," *IEEE Trans. Dielectr. Electr. Insul.*, vol. 25, no. 6, pp. 2467–2469, Dec. 2018.
[27] Y. Ohki and N. Hirai, "Spatial resolution between two abnormalities in a cable by frequency domain reflectometry," *IEEJ Trans. Electr. Electron. Eng.*, vol. 16, no. 6, pp. 822–826, Jun. 2021.
[28] D. K. Das-Gupta and P. C. N. Scarpa, "Modeling of dielectric relaxation spectra of polymers in the condensed phase," *IEEE Elect. Insul. Mag.*, vol. 15, no. 2, pp. 23–32, Mar. 1999.
[29] Q. Li, "Study on life assessment of cable group in pipes based on the operating temperature variation," M.S. thesis, Dept. Elect. Electron. Eng., Wuhan Univ., Wuhan, China, 2018.

MINGZHEN LI (Member, IEEE) was born in Xiangyang, Hubei, China, in 1991. He received the B.Sc. and Ph.D. degrees in electrical engineering from Wuhan University, China, in 2014 and 2019, respectively. He is currently a Lecturer with the School of Electrical Engineering, Nantong University. He is also a part-time Researcher with Wuhan University. His research interests include online monitoring and the condition assessment of electrical equipment.

RUIJUN YUAN, photograph and biography not available at the time of publication.

JIE CHEN, photograph and biography not available at the time of publication.

LIBIN HU, photograph and biography not available at the time of publication.

CHENYING LI, photograph and biography not available at the time of publication.

LINGZHI WANG, photograph and biography not available at the time of publication.

AOWEI GUO, photograph and biography not available at the time of publication.

ANLI CHEN, photograph and biography not available at the time of publication.

XINSONG ZHANG, photograph and biography not available at the time of publication.